

Modeling Optical Emissions from HE Fireballs

David Grote and Allen L. Kuhl
Lawrence Livermore National Laboratory
Livermore, California, USA

John B. Bell and Vincent E. Beckner
Lawrence Berkeley National Laboratory
Berkeley, California, USA

1 Introduction

In the past, we have studied combustion effects in confined explosions [1] and barometric calorimeters [2]. We have also studied the evolution of the evolution of turbulence fields in spherical combustion clouds [3]. And we have proposed gasdynamic models of turbulent combustion in TNT explosions [4]. Here we investigate optical emissions from fireballs created by the detonation of spherical high-explosives (HE) charges. The combustion field is modeled by the 3D gasdynamic conservation laws, integrated with a high-order Godonov scheme [4]; Adaptive Mesh Refinement (AMR) is used to capture the turbulent mixing structures on the computational mesh [5]. At each time-step, the flow field (of temperature, density and species) is fed into the 3D LUX code which does ray-tracing to compute the optical emissions of the fireball as a function of time. An example of a simulation of the fireball from a TNT explosion is compared with an experimental photograph in Fig. 1.

(a) 1-kg TNT Fireball



(b) 15-kg Comp B Fireball



Figure 1. Visualization of the optical emissions from HE fireballs: (a) AMR/LUX code simulations of a TNT fireball; (b) a frame from a high-speed video of a Comp B fireball.

2 Model

We consider an initial value problem starting at the time the detonation wave reaches the edge of the charge, so the detonation products are gases. We model the expansion of the detonation products and the ensuing blast waves that are created in the surroundings. We model the evolution of the combustion fields in the limit of large Reynolds and Peclet numbers, where effects of molecular diffusion and heat conduction are negligible. The flow field is then governed by the conservation laws of gasdynamics:

$$\begin{aligned}\partial_t \rho + \nabla \cdot (\rho \mathbf{u}) &= 0 \\ \partial_t \rho \mathbf{u} + \nabla \cdot (\rho \mathbf{u} \mathbf{u} + p) &= 0 \\ \partial_t \rho E + \nabla \cdot (\rho \mathbf{u} E + p \mathbf{u}) &= 0\end{aligned}$$

where ρ and p represent the gas density and pressure, \mathbf{u} is the velocity vector, $E = u + \mathbf{u} \cdot \mathbf{u} / 2$ is the total energy, and u is the specific internal energy.

We consider three components: TNT detonation products as fuel (F), air as oxidizer (A) and their equilibrium combustion products (P). We model the global combustion by $F + A \Rightarrow P$ so the mass fractions Y_k of the components are governed by the component conservation laws:

$$\begin{aligned}\partial_t \rho Y_F + \nabla \cdot \rho Y_F \mathbf{u} &= -\dot{s} \\ \partial_t \rho Y_A + \nabla \cdot \rho Y_A \mathbf{u} &= -\alpha \dot{s} \\ \partial_t \rho Y_P + \nabla \cdot \rho Y_P \mathbf{u} &= (1 + \alpha) \dot{s}\end{aligned}$$

Fuel and air are consumed in stoichiometric proportions: $\alpha = A / F$. In the above, \dot{s} represents the global kinetics sink term. In this work we use the fast-chemistry limit which is consistent with the inviscid gasdynamic model, so whenever fuel and air enter a computational cell, they are consumed in one time step.

Our code carries the density, specific internal energy and composition in each cell. These are used to calculate the pressure and temperature in a computational cell based on the following EOS model. The internal energy-temperature relation for component i ($i = F, A, P$) takes a quadratic form: $u_i(T) = a_i T^2 + b_i T + c_i$, where the constants $\{a_i, b_i, c_i\}$ were fit to Cheetah code [6] calculations of appropriate thermodynamic states. Pressure then comes from the perfect gas law: $p_i = \rho_i R_i T_i$. See [7] for more details.

The above conservation laws were integrated with a high-order Godunov scheme based on an efficient Riemann solver for gasdynamics [8] and extended to generalized conservation laws [9]. The Godunov scheme has been incorporated into an adaptive mesh refinement (AMR) algorithm that allows one to focus computational effort in complex regions of the flow such as mixing layers and reaction zones. Our adaptive methods are based on block-structured AMR algorithms [10], and extended to three-dimensional hyperbolic systems [11]. AMR is used to refine turbulent mixing regions; by successive refinements we are able to capture the energy-bearing scales of the turbulence on the computational grid—the so-called MILES approach of Jay Boris. Initially 8 levels of refinement were used.

We assume that the charge is consumed by a constant velocity Chapman-Jouguet (CJ) detonation wave. Therefore we initialize the computational grid with the self-similar flowfield corresponding to a spherical CJ detonation wave [12] when the detonation reaches the edge of the charge.

The ray-tracing model—the LUX code—uses a uniform cartesian mesh of cells: x_i, y_j, z_k , that contains the fireball. At selected times, the flow field (temperature, density and species) are mapped into that mesh, while the optical properties come from published data [13] and our soot model. For each cell

(j,k) , one starts at the $x=0$ plane and sums the emission and absorption irradiance from the relation:

$$I(j,k,t) = \sum_{i=1}^{i=l} (e_{ijk} - a_{ijk}), \text{ thereby producing an optical irradiance } I(j,k;t) \text{ at the plane } x_{\max}.$$

3 Results

A numerical simulation of the fireball created by the detonation of a 1-kg spherical TNT charge was performed. Visualizations of the temperature cross-section of the fireball and its associated optical irradiance are presented in Figs. 2 and 3. Figure 2 depicts the evolution of the fireball during the first optical peak. One can see the development of turbulent mixing structures on the fuel-air interface; combustion raises the local temperature to $\sim 2,500$ K (the adiabatic flame temperature). The strongest radiance comes from these combustion cells, producing bright mushroom-shaped structures seen in photography of fireballs in field tests (Fig. 1). As more air is entrained, the fireball cools, leading to a dimming of the fireball radiance (see frames 6 and 7 of Fig. 3). But the fireball contains an imploding shock, created by the over-expansion of the detonation products. After implosion, a second blast wave is formed that reheats the fireball—leading to a second optical pulse (frame 8, Fig. 3). Movies of these results will be presented in the lecture.

The time history of the optical radiance is depicted in Fig. 4; it clearly shows the first peak at $t_1 \sim 50 \mu\text{s} / \text{kg}^{1/3}$ and second peak at $t_2 \sim 3 \text{ms} / \text{kg}^{1/3}$. The spectral radiances at seven wavelengths: $\lambda_1 = 0.35264 \mu\text{m}$, $\lambda_2 = 0.40535 \mu\text{m}$, $\lambda_3 = 0.45267 \mu\text{m}$, $\lambda_4 = 0.56053 \mu\text{m}$, $\lambda_5 = 0.64379 \mu\text{m}$, $\lambda_6 = 0.75953 \mu\text{m}$, $\lambda_7 = 0.84638 \mu\text{m}$ were computed; results are shown in Fig. 5. The strongest radiance is in the long wavelengths λ_6 & λ_7 (the black and blue curves). The shorter wavelengths λ_1 & λ_2 (the red and purple curves) peak much earlier ($t \sim 50 \mu\text{s}$).

We have available the complete solution on each of the five grid levels; we chose the finest three levels and computed the spectral radiance histories $\lambda_i(t)$ at levels L_3, L_4, L_5 . Results are shown in Fig. 6. This illustrates the dependence of the most important part of the solution—spectral radiance—on grid resolution. Results for levels L_4 & L_5 are similar, indicating solution convergence.

References

- [1] Kuhl, AL, Reichenbach, H. (2009). Combustion effects in confined explosions, *Proc. Combustion Institute* **32** (2) pp. 2291-2298.
- [2] Kuhl, AL, Reichenbach, H. (2010). Barometric calorimeters, *Comb., Exp. & Shock Waves*, **4** (2) pp. 271-278.
- [3] Kuhl, AL, Bell, JB, Beckner, VE, Balakrishnan, K, Aspden, AJ. (2013). Spherical combustion clouds in explosions, *Shock Waves* **23** (3), pp. 233-249.
- [4] Kuhl, AL, Bell, JB, Beckner, VE, Reichenbach, H. (2011). Gasdynamic model of turbulent combustion in TNT explosions, *Proc. Combustion Institute* **33** pp. 2117-2185.
- [5] Bell, JB, Day, MS. (2011). Chapter 13: Adaptive methods for simulation of turbulent combustion, *Turbulent Combustion Modeling*, Fluid Mechanics and Its Applications **95**, Springer Media B, pp. 301-329.
- [6] Fried, L. (1995). Cheetah 1.22 User's Manual, **UCRL-MA-117541**, LLNL.
- [7] Kuhl, AL, Kasainov, B. (2007). Quadratic model of thermodynamic states in SDF explosions, *38th ICT*.
- [8] Collela, P., Glaz, HM. (1985). Efficient solution algorithms for the Riemann problem for real gases, *J. Comput. Phys.* **59**, pp. 164-289.
- [9] Bell, JB, Collela, P., Trangenstein, JA. (1989). Higher order Godunov methods for general systems of conservation laws, *J. Comput. Phys.* **92**(2), pp. 362-397.
- [10] Berger, MJ, Collela, P. (1989). Local adaptive mesh refinement for shock hydrodynamics, *J. Comput. Phys.* **82**(1), pp. 64-84.
- [11] Bell, JB, Berger, MJ, Saltzman, J, Welcome, M. (1994). A three-dimensional adaptive mesh refinement for hyperbolic conservation laws, *SIAM J. Sci. Stat. Comput.* **15**(1), pp. 127-138.
- [12] Kuhl, AL. (2015). On the structure of self-similar detonation waves in TNT charges, *Comb. Expl. & Shock Waves*, *50th Anniversary Issue* (in press).
- [13] Rothman, LS. et al (2009). The HITRAN 2008 molecular spectroscopic database, *J. Quant. Spectrosc. & Rad. Transfer* **110**, pp. 533-572.

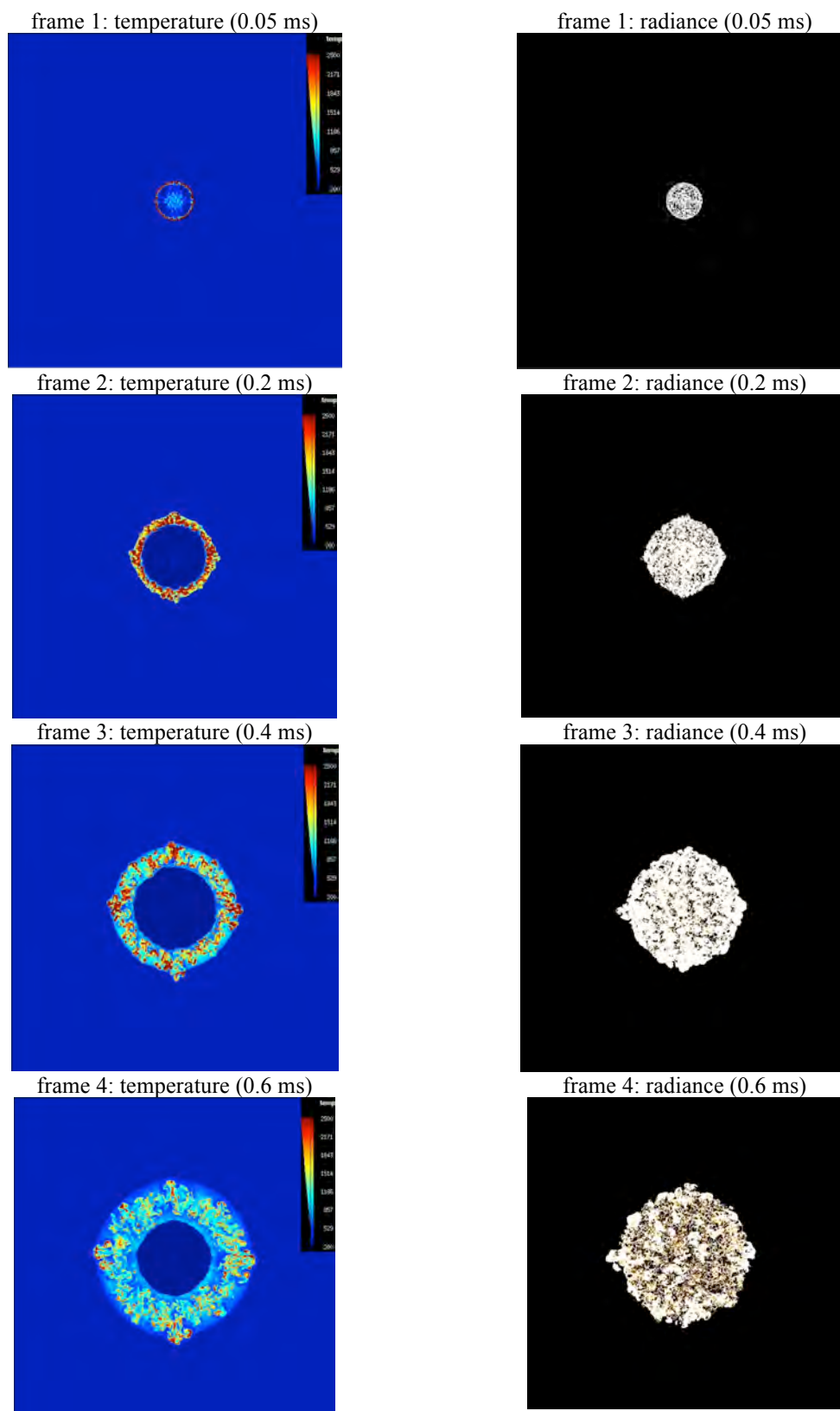


Figure 2. Evolution of the temperature cross-section and optical radiance (of soot) is shown during the first optical pulse. Note: detonation products are 43 mole % carbon graphite.

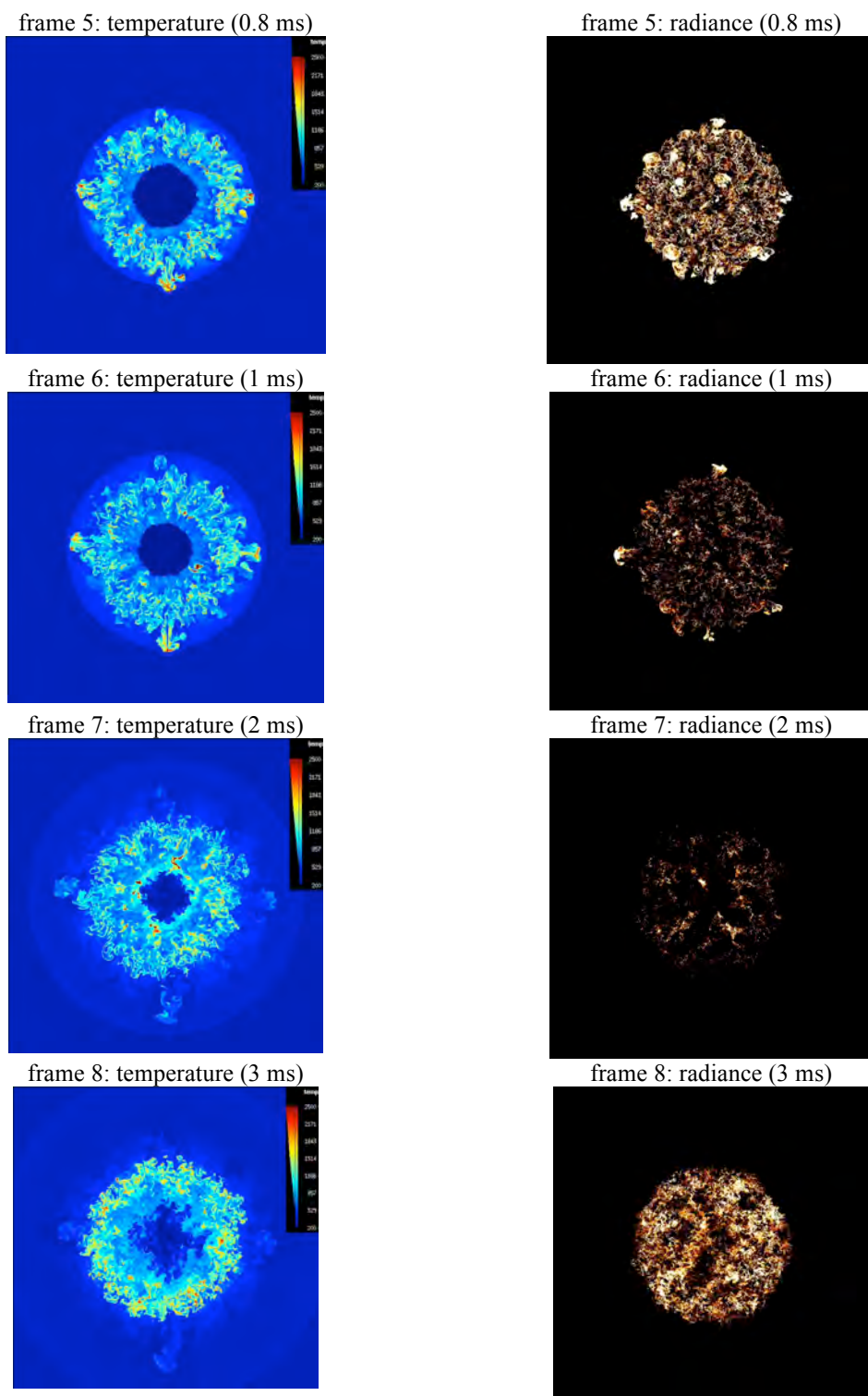


Figure 3. Evolution of the temperature cross-section and optical radiance (of soot) is shown during the cooling and then rebrightening (from the implosion shock) creating the second optical pulse. Note: detonation products are 43 mole % carbon graphite.

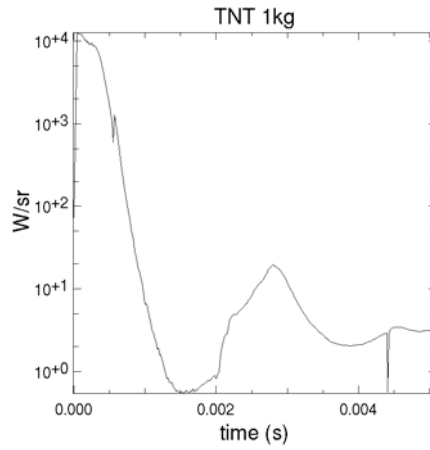


Figure 4. Computed radiance history (of soot) for 1-kg TNT charge.

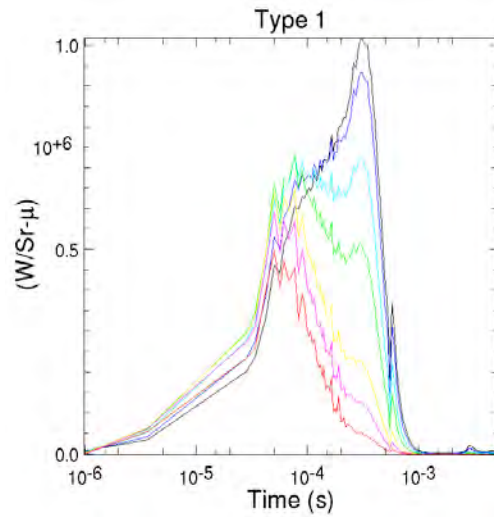


Figure 5. Computed radiance histories (of soot) at wavelengths λ_i for a 1-kg TNT charge. Wavelengths $\lambda_1 - \lambda_7$ correspond to black, blue, light-blue, green, yellow, purple and red curves, respectively.

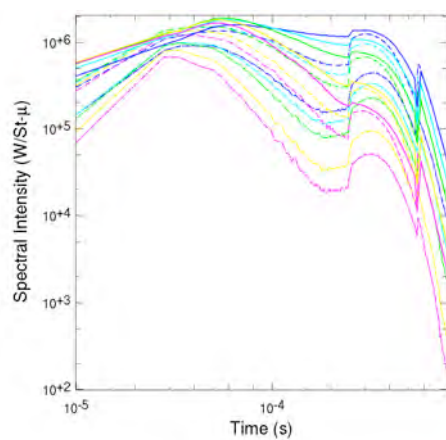


Figure 6. Comparison of spectral radiance (of soot) at different grid refinement levels. Color scheme is the same as Fig. 5; levels L_5, L_4 & L_3 correspond to solid, dashed and dotted curves, respectively.